J Appl Electrochem (2014) 44:399–410
DOI 10.1007/s10800-013-0642-2

RESEARCH ARTICLE

Single frequency electrochemical impedance investigation of zero charge potential for different surface states of Cu–Ni alloys

Benoît Ter-Ovanessian · Catherine Alemany-Dumont · Bernard Normand

Received: 22 July 2013 / Accepted: 21 October 2013 / Published online: 31 October 2013

Abstract Adsorption of sulphate anions onto polycrystalline pure copper, pure nickel and two copper–nickel alloys was explored by performing zero charge potential E_{PZC} measurements. E_{PZC} measurements were performed by differential capacitance analysis using single−frequency electrochemical impedance spectroscopy. E_{PZC} and surface charge of the studied materials were analysed for different surface states: bare—immediately after cathodic polarisation and after 5 h of immersion in a 0.1 M Na_2SO_4 solution. According to the surface state and nature of the studied materials, the choice of the appropriate measuring frequency was investigated. Specific methodologies dedicated to the study of electrode/electrolyte interfaces are then presented for bare metal, metals covered by corrosion products and metals covered by passive film. In the presence of passive film, the space charge capacitance interferes with the differential capacitance measurements, and its influence is discussed in the framework of semiconductor electrochemistry.

Keywords Potential of zero charge · EIS · Copper–nickel alloys · Interfaces · Passive films

B. Ter-Ovanessian (✉) · C. Alemany-Dumont · B. Normand
INSA de Lyon-MATEIS (UMR CNRS 5510)-Equipe CorrIS,
Bat Léonard de Vinci, 21 avenue Jean Capelle,
69621 Villeurbanne, France
e-mail: benoit.ter-ovanessian@insa-lyon.fr

C. Alemany-Dumont
e-mail: catherine.alemany-dumont@insa-lyon.fr

B. Normand
e-mail: bernard.normand@insa-lyon.fr

1 Introduction

The sustainability and integrity of metallic structural components are mainly due to the resistance of the constitutive materials to both uniform and localized corrosion. These resistances are most often correlated with the ability of those materials to form a thin protective oxide or, even better, a passive film [1, 2]. The efficiency and the durability of these layers are mainly governed by their nature, composition and structure [1–4].

Nevertheless, it is worth mentioning that oxide film properties and characteristics are themselves dependent on both material composition and the processes that govern their formation and growth [1–6]. It is commonly assumed that the applied physico-chemical conditions (environmental or electrochemical conditions occurring during these processes) are seminal factors in film construction. For example, adsorption and absorption of doping or detrimental species within the oxide layer are known to be mainly governed by these conditions and, more particularly, by the chemical species present in the electrolyte and the surrounding electrochemical environment. As insertion has direct consequences on oxide film properties, it seems essential to understand and assess adsorption mechanisms to predict film behaviour. Moreover, some oxide film degradation phenomena are known to be also related to the adsorption and penetration of aggressive species within films [7–12]. Halide ions, especially chloride ions Cl^-, are known to have detrimental effects on oxide or passive films. The adsorption of these species on the surface of films initiates localised film breakdown [8, 9]. It is expected that the nature, composition and structure of films have significant effects on halide ion adsorptions and consequently on the susceptibility of materials to localised corrosion [11]. Therefore, the adsorption mechanisms that

are active not only during film formation and growth but also in the steady state and during ageing must be characterised [12].

In the above context, the aim of this study is then to propose a methodology to assess the adsorption mechanism related to each step of the oxide film growth or ageing. It is well known that adsorption processes are correlated to the presence of surface charges at the material/electrolyte interface and are dependent on the electrode potential [13–15]. To understand the mechanism by which adsorption occurs, one of the experimental parameters most commonly used is the potential of zero charge (E_{PZC}) [13–16]. Assuming that at the E_{PZC} the excess charge at the electrode/electrolyte interface is eliminated, this potential is considered as a reference for determining the nature of surface charges [13–16]. In addition, the sign and the value of the difference (ΔE) between the electrode potential (commonly the stable value of open circuit potential, E_{OCP}) and E_{PZC} provides information about the type and the amount of ions adsorbed on an electrode surface. Different techniques are used to determine E_{PZC}: radiometric methods [17], friction methods [18], electrocapillary techniques [19, 20] or electrochemical impedance spectroscopy (EIS) techniques [21–27]. The measurement of the differential capacitance by EIS is currently one of the most commonly used methods, mainly onto single crystal/electrolyte interface [16, 24–27]. However, it required us to take into account some experimental precautions. The E_{PZC} determination effectively depends on the surface preparation of the sample and the surface structure as well as the pH of the solution and the electrolyte composition [13, 16, 20, 28]. Moreover, differential capacitance measurement also greatly depends on the choice of the measuring frequency [14, 22, 23]. This frequency selection is known to affect the accuracy of the results. In the present study, two surface conditionings performed on different copper–nickel (Cu–Ni) alloys were investigated by differential capacitance measurements: a bare surface (after cathodic polarisation) and a surface immersed in a 0.1 M Na_2SO_4 solution for 5 h. Consequently, particular attention has been paid to the selection of the frequency according to the nature of each tested surface to propose and establish an accurate investigating methodology by single−frequency EIS to apprehend the different adsorption processes.

2 Materials and experimental procedures

2.1 Materials and samples preparation

Samples were machined from two sheets of high-purity metals, Ni (Ni100) and Cu (Cu100), and from two sheets of commercial-grade Cu–Ni alloys, with 30 and 70 wt% Ni (named Ni30Cu70 and Ni70Cu30, respectively). The chemical compositions of these materials provided by Goodfellow Cambridge LTD were verified before test from EDX analysis.

Before each experiment, the specimen surfaces were mechanically ground with SiC paper and polished with diamond pastes down to 1 μm (mirror surface). After each preparation step, the coupons were ultrasonically cleaned in ethanol and pure water. The samples were then immediately transferred to an electrolytic cell.

2.2 Electrochemical measurements

Electrochemical measurements were performed on a conventional three-electrode cell outfitted with a GAMRY^{TM} Femtostat electrochemical system. Pure metals or Cu–Ni alloys were used as the working electrode (wall of the cell with a circular working area of 0.56 cm^2), while a graphite pin and a K_2SO_4−saturated mercury/mercurous sulphate electrode (E_{MSE} = 0.658 V/SHE) were used as the counter electrode and reference electrode, respectively. Electrochemical measurements were carried out in a naturally aerated sulphate solution (0.1 M Na_2SO_4, pH 6.9) at room temperature (23 ± 2 °C).

2.2.1 Determination of E_{PZC} of metals ($E_{PZC(bare)}$)

To remove the native oxide surface, cathodic polarisations were performed to freshly polished surfaces before the differential capacitance measurements. A preliminary study based on the evolution of the active peak area with the cathodic polarisation time was carried out to identify the best cathodic polarisation conditions for each material. For Cu100 and Ni30Cu70, a potential of −0.9 V/MSE was applied for 5 and 20 min, respectively, while Ni70Cu30 and Ni100 were cathodically polarised at −1.2 V/MSE for 20 and 30 min, respectively.

Immediately after polarisation, full EIS investigations were performed on bare metals at −0.9 V/MSE for the Cu100 and Ni30Cu70 alloys and at −1.2 V/MSE for the Ni100 and Ni70Cu30 alloys over frequencies ranging from 100 kHz to 0.01 Hz and at an applied AC disturbance signal of 8 mV RMS. From these EIS investigations, the frequencies domain of interest was determined to perform a relevant differential capacitances measurement.

Once the working frequency is chosen, differential capacitances were then measured through single-frequency EIS in potential ranging from −1.0 to +0.6 V/MSE with a potential step of 0.02 V on the materials freshly and cathodically polarised. An AC disturbance signal of 8 mV RMS was applied. From the single-frequency EIS measurement, the interfacial capacitance was estimated. Assuming that the interfacial capacitance is in this case the

double−layer capacitance (C_{dl}), the position of the minimum defined $E_{PZC(bare)}$.

2.2.2 *Determination of the E_{PZC} for the materials immersed for 5 h ($E_{PZC(ox)}$)*

After performing the cathodic polarisation mentioned above, the evolution of the open circuit potential of the each immersed sample was recorded over 5 h of immersion. In the following sections, E_{OCP} represents the corrosion potential obtained after this 5 h of immersion.

After 5 h of immersion, two different experiments were performed: potentiodynamic analysis and EIS measurement. Potentiodynamic polarisation curves were obtained at a scanning rate of 0.5 mV/s from −0.9 to 0.9 V/MSE. Electrochemical impedance measurements were performed at E_{OCP}, within the frequency ranging from 100 kHz to 0.01 Hz and at an applied AC disturbance signal of 8 mV RMS. Using these EIS results, the $E_{PZC(ox)}$ frequency was determined for each material. The frequency selection and the determination of $E_{PZC(ox)}$ are discussed in the Results section in terms of the nature of corrosion products (passive film, oxide film, etc.).

3 Results and discussion

3.1 $E_{PZC(bare)}$ measurements

Nyquist and Bode diagrams of the EIS measurements performed at the cathodic polarisation are reported in Fig. 1. First of all, the Nyquist plot (Fig. 1a) shows that, for the four materials, the EIS signal is unstable for frequencies ≤0.05 Hz. This is usually observed when EIS is performed at an applied potential in the cathodic domain. For this reason, only the signal above 0.05 Hz is fitted by the equivalent electrical circuit (EEC) presented in Fig. 1a. From the Bode plots of Cu100 (Fig. 1b), Ni30Cu70 (Fig. 1c), Ni70Cu30 (Fig. 1d) and Ni100 (Fig. 1e), two time constants related to physico-chemical phenomena may be defined. The first one, detected at low frequencies, is commonly associated with diffusion processes or some chemical reactions [29, 30]. In the present case, this diffusion process is suspected to occur for all materials at $f \leq 0.5$ Hz. In the case of the bare metals, the second time constant is related to the presence of an electrical double layer (C_{dl}) with a faradaic process (charge transfer resistance) [30] and may be considered as an equivalent R_tC_{dl} in parallel circuit. The faradaic current in the studied solution is due to hydrogen ions discharge or water decomposition [16]. To take into account the inhomogeneity of the surface and of the interface [31, 32], constant phase elements (CPE) were used in the EEC to fit the EIS results. The mathematical formulation of CPE is represented as follows:

$$Z_{CPE}(\omega) = \frac{1}{Q(j\omega)^{\alpha}} \quad (1)$$

For $\alpha = 1$, the CPE represents an ideal capacitor; for $\alpha = 0$, the CPE is an ideal resistor; for $\alpha = 0.5$, the CPE describes a Warburg impedance with diffusion character. In the EEC presented in Fig. 1a, CPE was used to describe the non-ideal capacitance of the double layer (Q_{dl}). Warburg impedance (Z_D) was used to describe the diffusion process. The calculated equivalent circuit parameters are displayed in Table 1. The Q_{dl} exponent α is close to 1, which indicates capacitance behaviour consistent with the presence of the double layer at the interface. Capacitance C_{dl} can be calculated from the Q_{dl} value using the Brug formula [33]. The values of the calculated C_{dl} are in agreement with conventional values of C_{dl} (commonly between approximately 15 and 50 μF cm^{-2}). According to this EIS analysis, the second shoulder (second intersection of the tangents) observed in the module plot ($f \approx 100$ Hz) may define the frequency domain in which the impedance measured is dominated more by the C_{dl} contribution than by the faradaic process [34]. Hence, the most relevant frequency range used to estimate C_{dl} was between 10 Hz (one decade less than 100 Hz) and 1,000 Hz (one decade more than 100 Hz). This frequency domain was investigated for each bare metal.

As similar behaviour was observed for the other materials, only the representative results obtained for the Ni70Cu30 alloy are shown in Fig. 2. For all of the tested frequencies, the evolution of the differential capacitance as a function of the applied potential presents a minimum value. As shown, the position and value of this minimum are slightly dependent on the frequency. First the measured C_{dl} decreases with increasing frequency, as already reported [22, 23]. Second the position shifts to cathodic values with increasing frequency probably due to the contribution of interfacial reactions like hydrogen adsorption/desorption due to the previous cathodic polarisation [16, 35]. For the lowest frequencies, the minimum capacitances measured are in agreement with the conventional values of C_{dl}. Moreover, at low frequencies, the curves are sharper and the minimum is better defined. Thus, the measurement frequency used to determine the $E_{PZC(bare)}$ of the bare metals must be between 10 and 50 Hz. In the following section, a frequency of 10 Hz was chosen to compare the four materials.

The evolution of the C_{dl} measured at 10 Hz on bare materials is shown in Fig. 3. $E_{PZC(bare)}$ globally shifts to cathodic values between Ni100 and Cu100. The values measured for Ni70Cu30 and Ni30Cu70 are quite similar. The presence of Ni in the Cu matrix modifies the charge

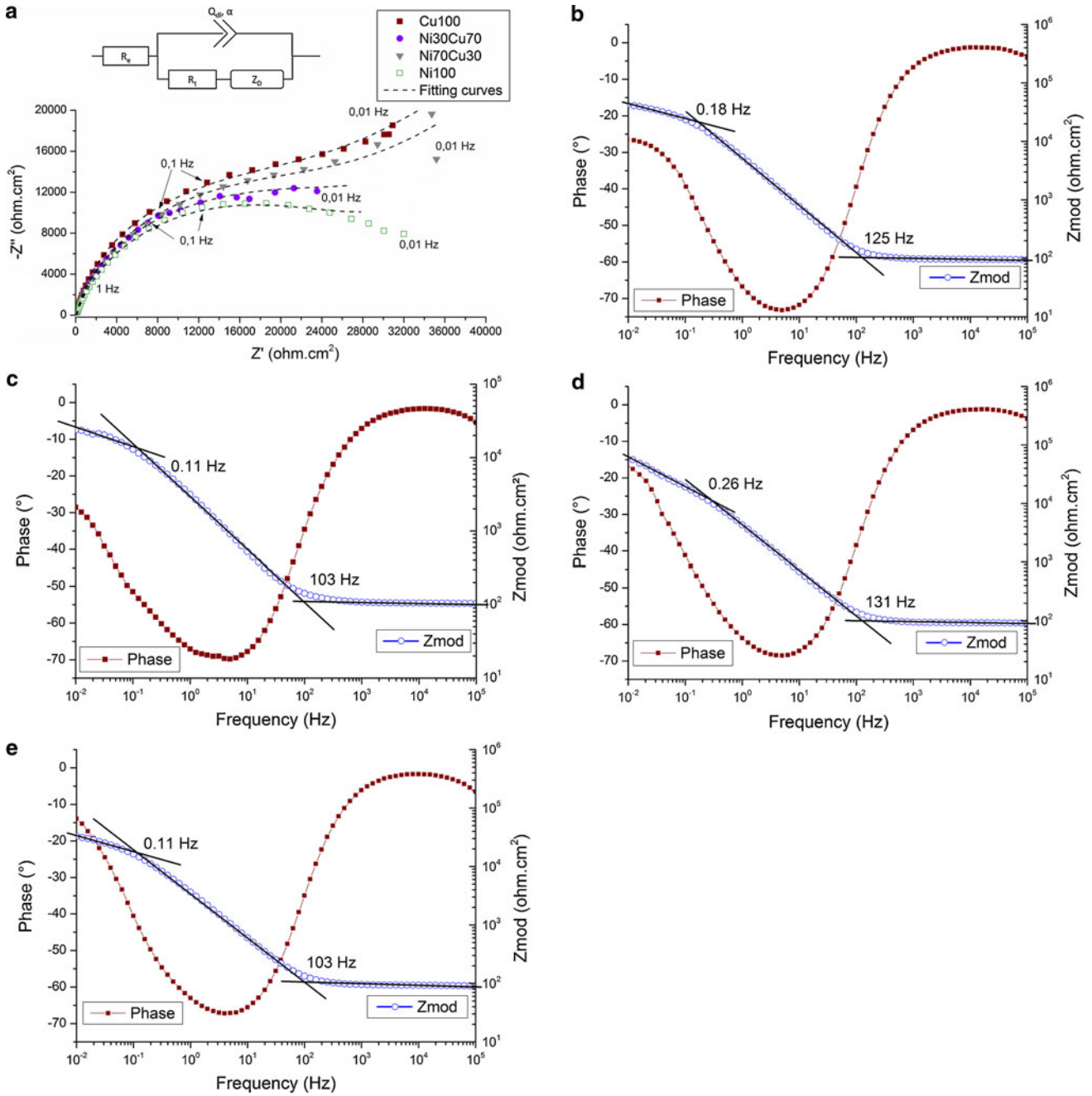

Fig. 1 Nyquist representation (**a**) and Bode plots from EIS measurements on bare materials (after cathodic polarisation) in 0.1 M Na_2SO_4 performed at −0.9 V/MSE for Cu100 (**b**) and Ni30Cu70 (**c**), at −1.2 V/MSE for Ni70Cu30 (**d**) and Ni100 (**e**). EEC used in the fitting of the impedance data (**a**): R_e electrolyte resistance, Q_{dl} constant phase element of the double layer, R_t charge transfer resistance, Z_D Warburg impedance

surface behaviour and then changes the adsorption behaviour of Cu–Ni alloys.

To determine the nature of the charge at the surface of the metal specimens, the potential of the metals and $E_{PZC(bare)}$ must be compared. The potentials measured after 5 h of immersion as well as the C_{dl} and $E_{PZC(bare)}$ values are reported in Table 2, and Fig. 4 shows the evolution of the potential over the immersion time. At the beginning of the immersion, the potentials measured for the four materials are more negative than $E_{PZC(bare)}$, suggesting that the metal surfaces are negatively charged. During this stage, the electrolyte is mainly composed of water molecules, SO_4^{2-} anions and solvated Na^+ cations. Some discharge of hydrogen ions may also occur at cathodic potentials which suggest that the pH locally differs. Such hydrogen evolution may have an impact on the E_{PZC} determination

Table 1 Equivalent circuit parameters for the studied materials from EIS performed atzapplied potentials: −1.2 V/MSE for Ni100 and Ni70Cu30, −0.9 V/MSE for Ni30Cu70 and Cu100

	Cu100	Ni30Cu70	Ni70Cu30	Ni100
R_e (Ω cm^2)	95.54	91.78	89.77	89.21
Q_{dl} (μF s$^{\alpha-1}$ cm^{-2})	32.86	52.50	46.29	56.86
α	0.897	0.829	0.845	0.831
C_{dl} (μF cm^{-2})	31.79	47.70	54.86	60.89
R_t (Ω cm^2)	22,839	23,576	25,448	24,640
W (Ω cm^2 s$^{-1/2}$)	5,752.88	3,612.00	3,838.80	1,729.28

Capacitance C_{dl} is calculated from the Q_{dl} value using the Brug formula [33]

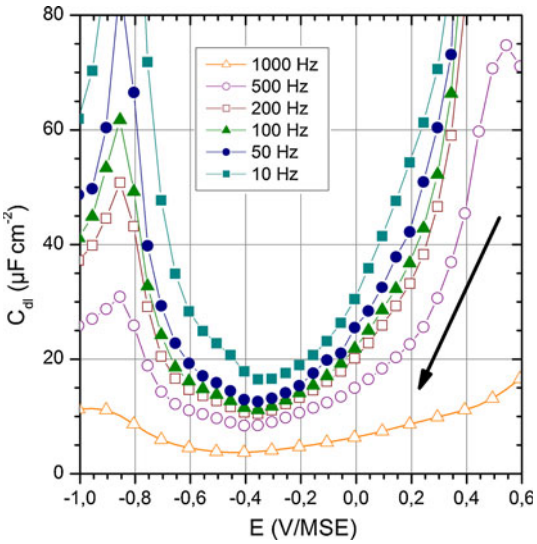

Fig. 2 Relationship between double−layer capacitance and applied potential as a function of the measuring frequency for Ni70Cu30 alloy after cathodic polarisation (bare metal)

[16, 35]. However, in the present case, the pH dependence seems not sufficient to modify the sign of the surface charge. As the surface is negatively charged, only cations (Na^+, H^+) or solvent dipoles are suspected to be adsorbed, and the preferential adsorption of anions at the metal surface is not expected during the first stages of oxidation [13]. Metallic cations are generally solvated in neutral aqueous solution, meaning that their adsorptions is not favoured [36, 37]. This result is in agreement with the oxide film growth mechanism proposed by Okamoto [38]. Indeed, Okamoto supposed that a layer of adsorbed water molecules at the surface of a metal is the first step of the oxide film formation. Moreover, Okamoto assumed that the subsequent metal dissolution and deprotonation of the adsorbed water molecules occur simultaneously to form a passive film [3, 38].

The difference between the potential of the electrode and $E_{PZC(bare)}$ decreases as the immersion time increases,

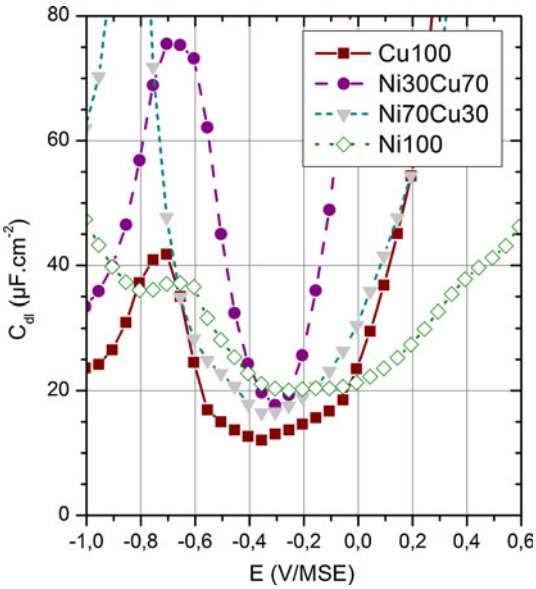

Fig. 3 Determination of $E_{PZC(bare)}$ for the four studied materials just after the cathodic polarisation (10 Hz)

Table 2 Minimum values of the interfacial double layer C_{dl} and of $E_{PZC(bare)}$ measured for the studied materials immediately after cathodic polarisation

	Cu100	Ni30Cu70	Ni70Cu30	Ni100
$C_{dl\ (minimum)}$ (μF cm^{-2})	12.7	17.9	16.7	20.2
$E_{PZC(bare)}$ (V/MSE)	−0.369	−0.315	−0.325	−0.215
E_{OCP} (V/MSE)	−0.472	−0.441	−0.413	−0.356

The open-circuit potential E_{OCP} determined after 5 h of immersion is also reported

reaching a minimum when the stationary state is reached. However, it is worth mentioning that the formation of an oxide film during the immersion implies changes at the electrode/electrolyte interface in terms of reactivity and surface charge distribution. Consequently, the E_{PZC} measured on bare surfaces must be not considered as a reference potential for the study of the adsorption mechanisms that occur on oxidised materials. Therefore, the E_{PZC} of oxidised materials must be determined ($E_{PZC(ox)}$).

3.2 $E_{PZC(ox)}$ measurements on materials after 5 h of immersion

During immersion, the behaviour of the electrode/electrolyte interface greatly depends on the nature and the amount of the corrosion products. To determine the surface state, potentiodynamic studies were performed before the determination of $E_{PZC(ox)}$. The polarisation curves obtained for all materials investigated in this study are plotted in Fig. 5. Focusing on the anodic part of the polarisation curves,

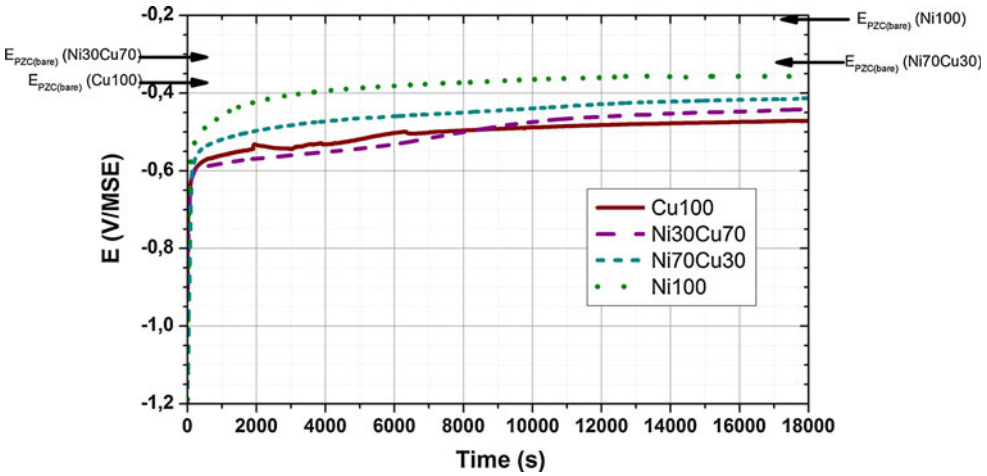

Fig. 4 Open−circuit potential measurements obtained after the cathodic polarisation of the four studied materials

passive behaviour was observed for Ni100 over a wide potential domain. Conversely, for the material containing mainly Cu, Cu100 and Ni30Cu70, the corrosion behaviour is defined by the formation of corrosion products, which slightly limit the diffusion phenomena, and by the significant general dissolution that occurs beyond anodic overpotentials of 0.170 and 0.223 V for Cu100 and Ni30Cu70, respectively. Alloy Ni70Cu30 exhibits intermediate behaviour, featuring an active peak and a pseudo-passive plateau, proving that the addition of Cu reduces the ability to form a stable and an efficient barrier film. These results indicate that three main corrosion behaviours may be observed for the studied materials: the formation of corrosion products precipitated at the surface, the formation of an oxide film and the formation of a passive film. The observation of these three behaviours is concomitant with the literature [39–43].

In the following section, Ni100, as the only material forming a passive film characterised by a specific electrochemical behaviour, was studied separately from the other materials.

3.2.1 $E_{PZC(ox)}$ measurements for the oxidised Cu100, Ni30Cu70 and Ni70Cu30

To optimise the frequency used for the $E_{PZC(ox)}$ determination, EIS measurements were performed at the E_{OCP} of the 5−h-immersed materials. Nyquist and Bode diagrams of the EIS measurements are reported in Fig. 6. The three materials exhibit distorted capacitive loops on the Nyquist plot (Fig. 6a), suggesting that different contributions occur in similar frequency domains. From the shape of the Bode plots of Cu100 (Fig. 6b), Ni30Cu70 (Fig. 6c) and Ni70Cu30 (Fig. 6d), three overlapped time constants, indicating three physico-chemical contributions, may be assumed. As previously mentioned, the existence of the low-frequency time constant is related to diffusion

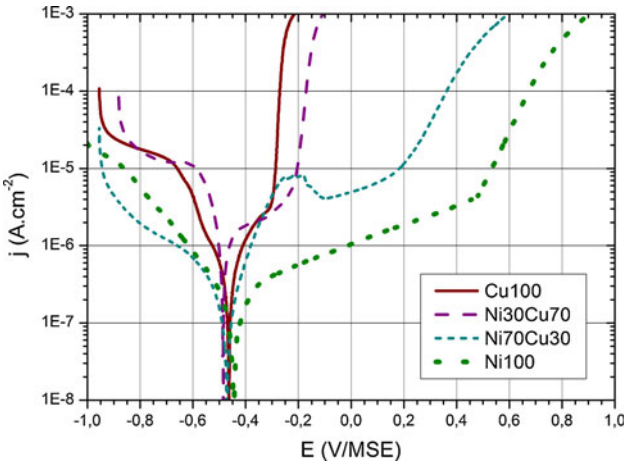

Fig. 5 Polarisation curves obtained for the four materials after 5 h of immersion in 0.1 M Na_2SO_4

processes. In the present case, either diffusion within the oxide film or oxygen diffusion/convection in the electrolyte is suspected to occur in all of the materials. The diffusion process is then characterised by frequencies below 0.060, 0.049 and 0.065 Hz (first shoulder of the module plots) for Cu100, Ni30Cu70 and Ni70Cu30, respectively. However, the Nyquist plot indicates that the EIS spectra performed up to 0.01 Hz is not sustaining to define totally this time constant. Consequently, the EEC used to fit the results of the oxidized materials (Fig. 6a) does not take into account precisely these diffusion processes. The two other measured contributions are identified to represent the oxide film (film capacitance and film resistance, equivalent R_fC_f in parallel circuit) associated in parallel with the parallel association of C_{dl} with the charge transfer resistance (as observed for bare metals). The shapes of the Bode plots (module and phase) indicate that these two phenomena are conjointly measured by EIS. On the EEC presented on Fig. 6a, CPE were used for define both capacitances (Q_{dl} and Q_f). The fitting parameters are reported in Table 3. The

Q_f exponent α is close to 1, which indicates capacitance behaviour of the oxide film, while the Q_{dl} exponent α is about 0.5, suggesting that the double layer is disturbed by diffusion process at low frequency. The increases of the film resistance and of the charge transfer resistance with the increase of Ni content indicate that the incorporation of Ni in copper oxides improves the protectiveness of these oxide films. These results are concomitant with the results observed on potentiodynamic curves.

From the EIS analysis, it is possible to assume that high frequencies are related to the oxide film contribution. The third intersection of the modules' tangents may be considered to determine the frequency domain over which the measured impedance is dominated by the oxide film capacitance response. Hence, to minimise the contribution of the oxide film to the differential capacitance measurement, the frequency must be selected from within the intermediate frequency domain (strictly below 315 Hz for Cu100 and for Ni30Cu70 or below 228 Hz for Ni70Cu30). Moreover, the measuring frequency must also be chosen from within the frequency domain where the charge transfer contribution is limited and where the C_{dl} contribution is maximal. Thus, the selected frequency must be equal to or above 10–50 Hz (about one order of magnitude greater than the second intersection of the modules' tangents). In the present study, a frequency of 10 Hz was chosen to determine the $E_{PZC(ox)}$ and to compare this value to $E_{PZC(bare)}$.

The variations of the differential capacitances with the applied potential for the materials immersed in 0.1 M Na_2SO_4 for 5 h are compared with the results obtained on

Table 3 Equivalent circuit parameters (EEC on Fig. 6a) for Cu100, Ni30Cu70 and Ni70Cu30 from EIS performed at E_{OCP}

	Cu100	Ni30Cu70	Ni70Cu30
R_e (Ω cm^2)	90.22	81.26	85.40
Q_f (μF s$^{\alpha-1}$ cm^{-2})	6.06	20.80	17.43
α_1	0.931	0.880	0.912
R_f (Ω cm^2)	6,460	4,004	19,351
Q_{dl} (μF s$^{\alpha-1}$ cm^{-2})	62.54	76.91	29.05
α_2	0.575	0.497	0.602
R_t (Ω cm^2)	27,241	72,486	155,436

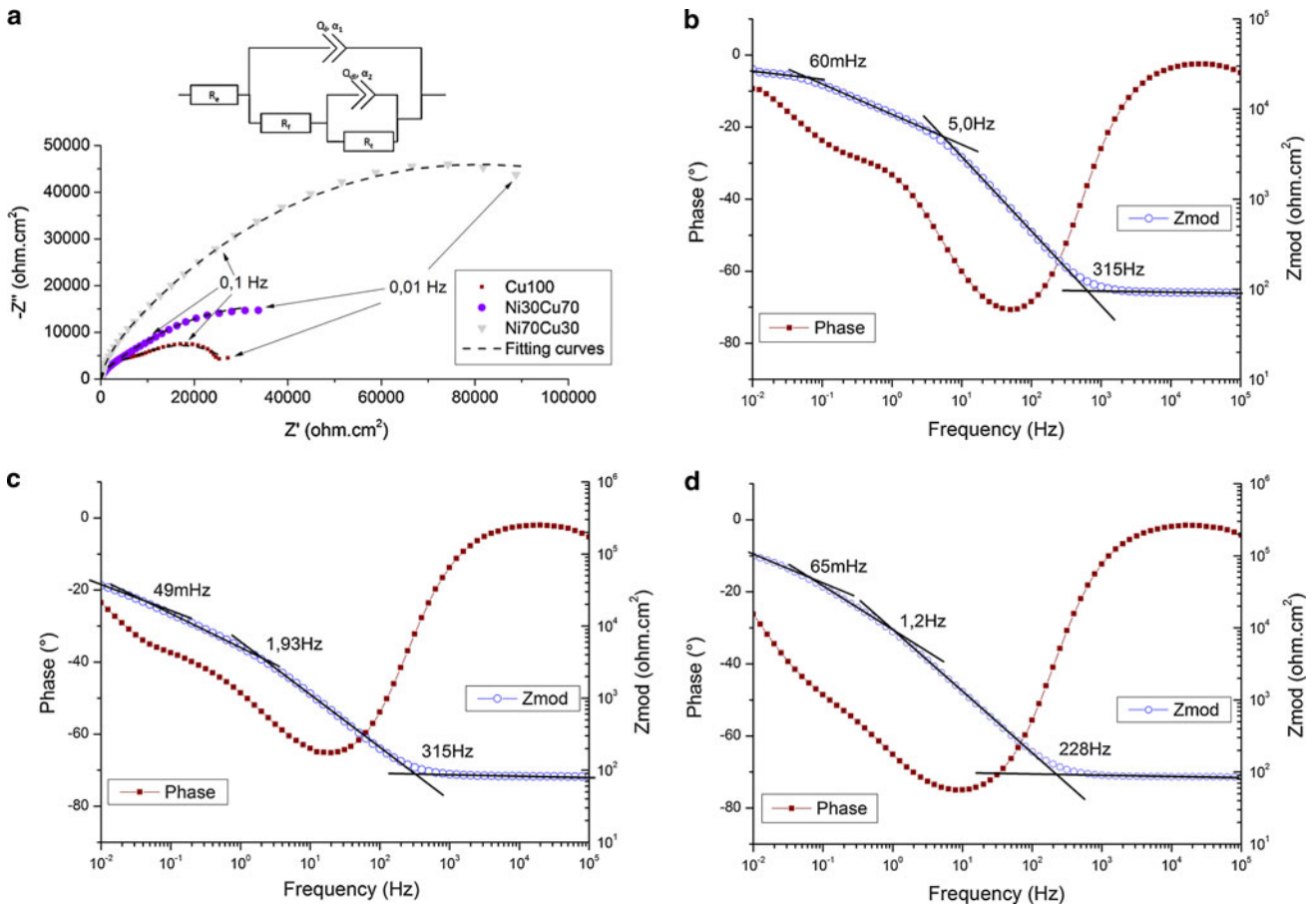

Fig. 6 Nyquist representation (**a**) and Bode plots from EIS measurements on materials exposed to 0.1 M Na_2SO_4 for 5 h: Cu100 (**b**), Ni30Cu70 (**c**) and Ni70Cu30 (**d**). EEC used in the fitting of the impedance data (**a**): R_e electrolyte resistance, Q_f constant phase element of the oxide film, R_f oxide film resistance Q_{dl} constant phase element of the double layer, R_t charge transfer resistance

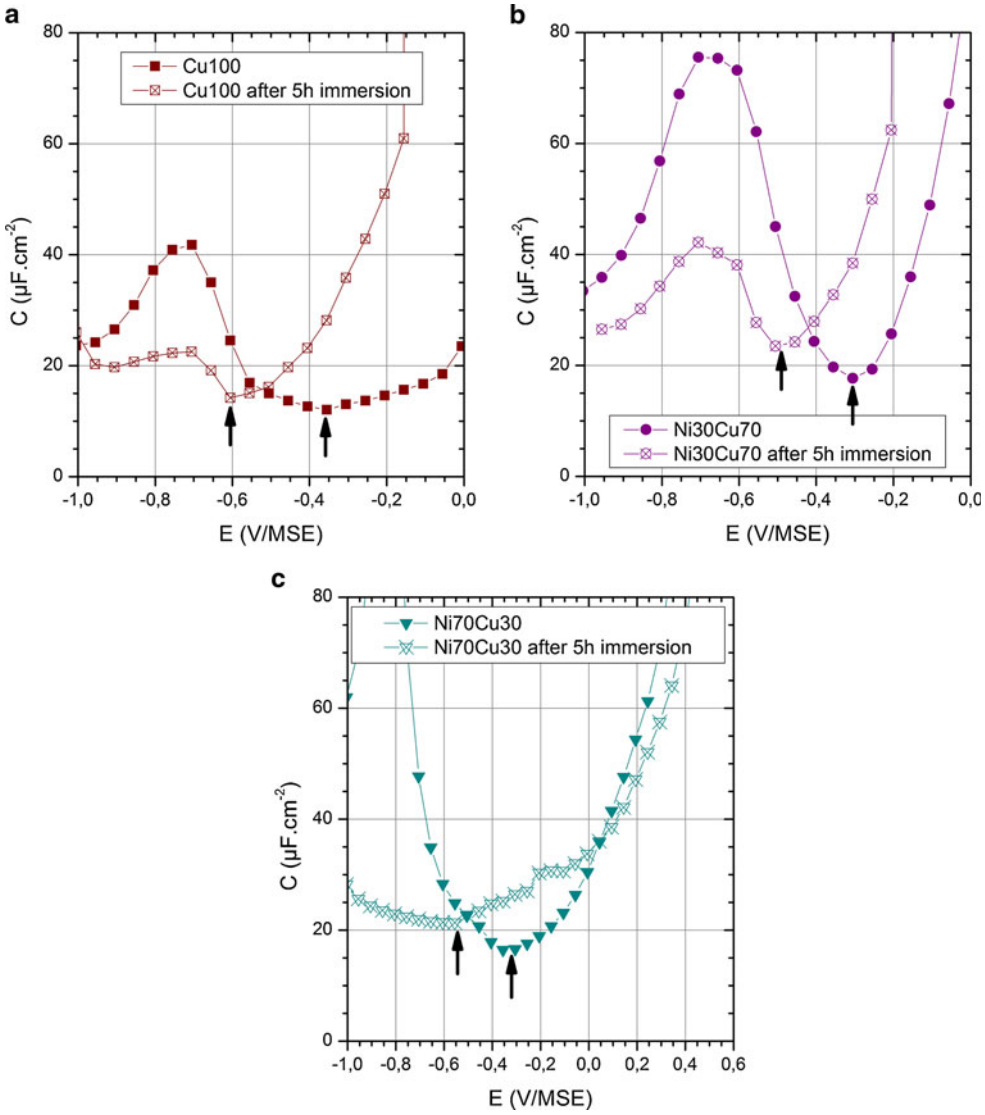

Fig. 7 Evolutions of the differential capacitance versus applied potential for bare materials and materials immersed for 5 h for Cu100 (**a**), Ni30Cu70 (**b**) and Ni70Cu30 (**c**). Experiments were performed at 10 Hz

bare metals in Fig. 7. First, for Cu100 (Fig. 7a), Ni30Cu70 (Fig. 7b) and Ni70Cu30 (Fig. 7c), the differential capacitances measured for the oxidised material remain on the same order of magnitude as the value obtained for the bare materials, which indicates that the choice of this frequency is appropriate. Second, all the differential capacitances were always slightly higher for the oxidised materials than for the bare ones. This suggests that the capacitive behaviour of the oxide film effectively and slightly contributes to the differential capacitance measurement at this frequency or that the presence of the oxide film affects the nature of electrical double layer formed. The method used in the present study does not allow for the issue between these two assumptions. Third, the $E_{PZC(ox)}$ measured on the oxidised materials are more cathodic than the bare materials oxidised ones. The differences between E_{OCP} and $E_{PZC(ox)}$ ($\Delta E_{(ox)} = E_{OCP} - E_{PZC(ox)}$) are reported in Table 4. In the presence of an oxide layer at the electrode surface, $\Delta E_{(ox)}$ showed positive values for the three materials mentioned, suggesting that after 5 h of immersion, the electrode was positively charged at E_{OCP}. From these results, the preferential adsorption of anions (SO_4^{2-}) is assumed to occur at the surface of the oxide film. Such SO_4^{2-} adsorption has been experimentally observed on Copper [44, 45] and Cu–Ni alloys [42, 46]. Furthermore, it seems possible that these adsorbed anions participate either

Table 4 Values of the minimum of the interfacial double layer C_{dl} and of $E_{PZC(ox)}$ measured on the studied materials immediately after 5 h of immersion

	Cu100	Ni30Cu70	Ni70Cu30
$C_{dl\ (minimum)}$ (µF cm^{-2})	13.9	23.2	21.4
$E_{PZC(ox)}$ (V/MSE)	−0.605	−0.495	−0.527
E_{OCP} (V/MSE)	−0.472	−0.441	−0.413
$\Delta E_{(ox)}$ (V)	+0.133	+0.054	+0.114

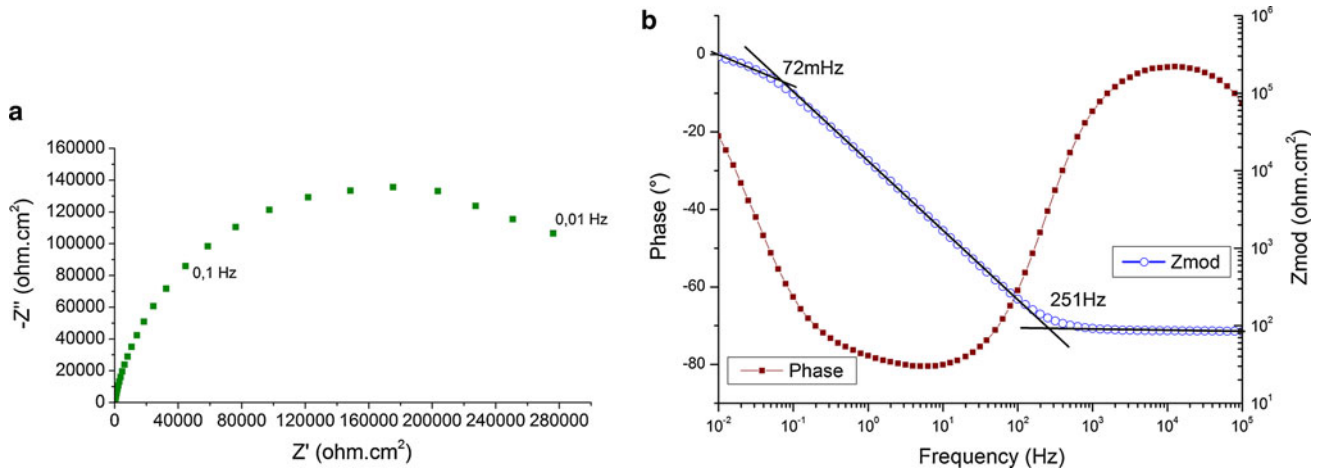

Fig. 8 Nyquist (**a**) and Bode (**b**) plots from EIS measurements on Ni100 exposed to 0.1 M Na_2SO_4 for 5 h

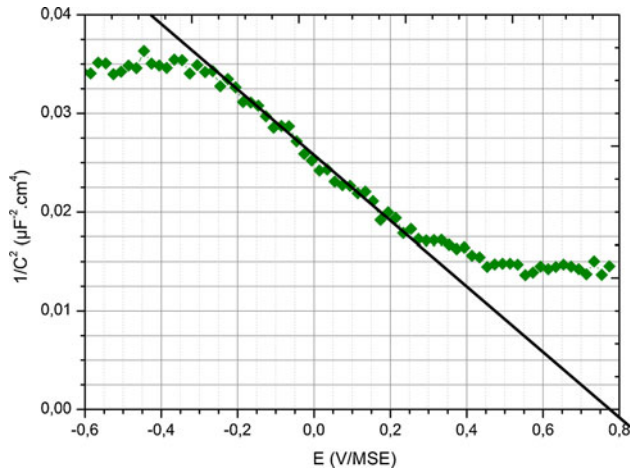

Fig. 9 Mott–Schottky relationship of passive Ni100 (5 h of immersion) obtained at 5,000 Hz

in the formation or in the maturation of the oxide layer. Some studies on Cu–Ni alloys in sulphate solutions have established the existence of a critical sulphate concentration above which the corrosion resistance increases, suggesting that SO_4^{2-} contributes to the barrier effect of the oxide [42, 46]. These results confirm the occurrence of SO_4^{2-} adsorption during the formation of the corrosion products and oxide film on Cu and Cu–Ni as predicted by the single−frequency differential capacitance measurement on oxidised surface.

3.3 '$E_{PZC(ox)}$' measurements for a passive material Ni100

As shown in Fig. 8, the EIS measurements performed on Ni100 after 5 h of immersion indicate that Ni100 behaves like a passivable material in sulphate solution which is consistent with numerous works on nickel passivity [47–50]. The Nyquist plot (Fig. 8a) exhibits a single distorted capacitive loop, while on the Bode diagram (Fig. 8b), two time constants are observed. These overlapped time constants are consistent with the presence of a passive film exhibiting semiconducting properties (space charge region) and with the occurrence of migration within the passive film [51]. The space charge region is located within the passive film in the vicinity of the passive film/electrolyte interface [3, 29]. The presence of this space charge region has an influence on the interfacial system, and the space charge region must be considered jointly with the interfacial double layer when the E_{PZC} is studied on passive metals. Indeed, both regions present capacitive behaviours, which must be taken into account when differential capacitance measurements are performed. The relationship between the measured differential capacitance and the global capacitance of both regions may be expressed as follows [52, 53]:

$$1/C = 1/C_{dl} + 1/C_{sc} \quad (2)$$

where C is the measured differential capacitance, C_{dl} the interfacial double layer capacitance and C_{sc} the space charge capacitance. In this study, C_{sc} was lower than C_{dl} (often $C_{dl} \gg C_{sc}$), indicating that the measured capacitance C is mainly determined by C_{sc} [52]. Furthermore, the presence of the space charge region modifies the controlling mechanism of the electrode/electrolyte interface system [52–55]. Surface charges are therefore mainly governed by the properties of the space charge region. Thus, E_{PZC} is defined by the potential at which there is no band bending in the space charge region due to charges′ accumulation at the surface of the passive film [15]. This E_{PZC}, resulting from the electrochemistry of semiconductor theory, is commonly called the flat band potential, E_{fb}. E_{fb} can be measured from

impedance analysis. Indeed, if it is possible to consider only the C_{sc}, then the capacitance of a semiconducting passive layer obeys the Mott–Schottky relationship [15, 47, 53–55]:

$$1/C^2 = \frac{2}{e\varepsilon\varepsilon_0 N} \cdot \left(E - E_{fb} - \frac{kT}{e}\right) \quad (3)$$

where e is the electron charge (1.6×10^{-19} C), ε is the relative dielectric constant of the oxide, ε_0 is the vacuum permittivity (8.85×10^{-14} F cm^{-1}), N is the carrier density, k is the Boltzmann constant (1.38×10^{-23} J K^{-1}), T is the absolute temperature, E_{fb} is the flat band potential and E is the applied potential. E_{fb} is obtained from the extrapolation of the linear relationship between E and $1/C^2$ to $1/C^2 = 0$. Therefore, Mott–Schottky experiments were performed to determine E_{fb} of passive Ni100. As previously mentioned, the frequency selected for this analysis must be higher than the characteristic frequencies of the reactions linked to redox species present in the solution and must be the only frequency characteristic of the semiconducting passive layer. Moreover, if the capacitance measured is still a function of frequency even at high frequencies, the value E_{fb} determined by Mott–Schottky analysis is commonly considered to be independent of the applied frequency [56, 57]. Hence, the frequency used for the Mott–Schottky analysis was fixed at 5 kHz.

Figure 9 shows the Mott–Schottky curve obtained for Ni100 after 5 h of immersion. The negative slope observed in the linear part of the curve indicates that the passive film formed on Ni100 behaved like a p-type semiconductor, which is in agreement with the results of the previous studies [47, 48]. The measured E_{fb} value is +0.781 V/MSE, and the difference between E_{OCP} (−0.356 V/MSE) and E_{fb} is −1.137 V. These results suggest that at E_{OCP} the space charge is in depletion (p-type semiconductor), and the surface of the passive film is negatively charged. In the case of Ni100, the passive film prevents SO_4^{2-} adsorption. Consequently, in a neutral sulphate solution, SO_4^{2-} ions are suspected to neither contribute to the passivation process nor disturb it during passive film formation as well as in the steady-state passive film regime. However it is worth mentioning that passive film is often described as duplex: an inner dense oxide layer and an outer hydrated oxo-hydoryde layer [58, 59]. The behaviour of the outer layer on adsorption remains under question and further works are required to determine the potential role of the hydrated layer on anions adsorption on passive film.

4 Conclusion

E_{PZC} determination by single−frequency EIS is a relevant electrochemical method to assess the role of anions′ adsorption on the corrosion behaviour of materials. However, as evidenced in the present work, particular precautions are required in the determination of the working frequency regarding to the electrode/electrolyte state.

In this study on different Ni–Cu alloys behaviour and on different surface conditionings, three statements are demonstrated:

- The adsorption of SO_4^{2-} ions was expected to occur only on oxidised Cu100, Ni30Cu70 and Ni70Cu30 materials. Some authors effectively prove such adsorption phenomenon on these materials.
- All bare metals exhibited a more anodic E_{PZC} than the reached E_{OCP} in a 0.1 M Na_2SO_4−aerated solution, suggesting that within this concentration, SO_4^{2-} most likely does not participate during the first stages of oxidation but only after the formation of a critical amount of corrosion product. The determination of this critical amount deserves further investigation.
- Finally, for Ni100, the passive film surface is negatively charged at E_{OCP}, preventing anions′ adsorption. Furthermore, this work confirms that for passive materials, the adsorption mechanism is governed mainly by the space charge region of the passive film.

References

1. Tomashov ND (1964) Passivity and corrosion resistance of metal systems. Corros Sci 4:315–334
2. Macdonald DD (1999) Passivity—the key to our metals-based civilization. Pure Appl Chem 71:951–978
3. Sato N (1990) An overview on the passivity of metals. Corros Sci 31:1–19
4. Schmuki P (2002) From Bacon to barriers: a review on the passivity of metals and alloys. J Solid State Electrochem 6:145–164
5. Marcus P (1994) On some fundamental factors in the effect of alloying elements on passivation of alloys. Corros Sci 36:2155–2158
6. Lavigne O, Alemany-Dumont C, Normand B, Delichere P, Descamps A (2010) Cerium insertion in 316L passive film: effect on conductivity and corrosion resistance performances of metallic bipolar plates for PEM fuel cell application. Surf Coat Technol 205(7):1870–1877
7. Martin FJ, Cheek GT, O'Grady WE, Natishan PM (2005) Impedance studies of the passive film on aluminium. Corros Sci 47:3187–3201
8. Lin LF, Chao CY, Macdonald DD (1981) A point defect model for anodic passive films II. Chemical breakdown and pit initiation. J Electrochem Soc 128:1194–1198
9. Li DG, Feng YR, Bai ZQ, Zhu JW, Zheng MS (2007) Influence of temperature, chloride ions and chromium element on the electronic property of passive film formed on carbon steel in bicarbonate/carbonate buffer solution. Electrochim Acta 52:7877–7884
10. Mankowski G, Duthil JP, Giusti A (1997) The pit morphology on copper in chloride- and sulphate-containing solutions. Corros Sci 39:27–42
11. Liu Y, Meng GZ, Cheng YF (2009) Electronic structure and pitting behavior of 3003 aluminum alloy passivated under various conditions. Electrochim Acta 54:4155–4163

12. Marcus P, Herbelin JM (1993) The entry of chloride ions into passive films on nickel studied by spectroscopic (ESCA) and nuclear (36Cl radiotracer) methods. Corros Sci 34:1123–1145
13. Damaskin BB, Petrii O (2011) Historical development of theories of the electrochemical double layer. J Solid State Electrochem 15:1317–1334
14. Larios-Duran ER, Antano-Lopez R, Keddam M, Meas Y, Takenouti H, Vivier V (2010) Dynamics of double-layer by AC modulation of the interfacial capacitance and associated transfer functions. Electrochim Acta 55:6292–6298
15. McCafferty E (2010) Relationship between the isoelectric point (pHpzc) and the potential of zero charge (Epzc) for passive metals. Electrochim Acta 55:1630–1637
16. Lukomska A, Sobkowski J (2004) Potential of zero charge of monocrystalline copper electrodes in perchlorate solutions. J Electroanal Chem 567:95–102
17. Balashowa N, Kazarinov V (1969) Electroanalytical chemistry, vol 3. Marcel Dekker, New York
18. Leikis D, Panin V, Rybalka R (1972) On the measurement of the electric double layer capacity at a polycrystalline cadmium electrode. J Electroanal Chem 40:9–12
19. Bockris JO'M, Argade SD (1969) Dependence of friction at wet contacts upon interfacial potential. J Chem Phys 50:1622–1623
20. Grahame DC (1947) The electrical double layer and the theory of electrocapillarity. Chem Rev 41:441–501
21. Fredlein R, Bockris JO'M (1974) Electrocapillary study of gold-perchloric acid solution interface. Surf Sci 46:641–652
22. Bockris JO'M, Argade SD, Gileadi E (1969) The determination of the potential of zero charge on solid metal. Electrochim Acta 14:1259–1283
23. Leikis DI, Rybalka KV, Sevastyanov ES, Frumkin AN (1973) Determination of the potentials of zero charge of solid metals by means of differential capacity measurements. Electroanal Chem Interface Electrochem 46:161–169
24. Hamelin A, Vitanov T, Sevastyanov E, Popov A (1983) The electrochemical double layer on sp metal single crystals: the current status of data. J Electroanal Chem 145:225–264
25. Valette G (1981) Double layer on silver single-crystal electrodes in contact with electrolytes having anions which present a slight specific adsorption: part I. The (110) face. J Electroanal Chem 122:285–297
26. Bachetta M, Trasatti S, Doubova L, Hamelin A (1986) The dependence of the potential of zero charge of silver electrodes on the crystallographic orientation of the surface. J Electroanal Chem 200:389–396
27. Jovic VD, Jovic BM (2003) EIS and differential capacitance measurements onto single crystal faces in different solutions: part II: Cu(111) and Cu(100) in 0.1 M NaOH. J Electroanal Chem 541:13–21
28. Devanathan MAV, Tilak BVKSRA (1965) Structure of electrical double layer at metal–solution interface. Chem Rev 65:635–684
29. Beranger G, Dabosi F, Baroux B (1994) Corrosion localisée. EDP Sciences, Paris
30. Bockris JO'M, Khan SUM (1993) Surface electrochemistry. Plenum Press, New York
31. Lukacs Z (1999) Evaluation of model and dispersion parameters and their effects on the formation of constant-phase elements in equivalent circuits. J Electroanal Chem 464:68–75
32. Macdonald JR (1985) Generalizations of "universal dielectric response" and a general distribution-of-activation-energies model for dielectric and conducting systems. J Appl Phys 58:1971–1978
33. Brug GJ, Van den Eeden ALG, Sluyters-Rehhbach M, Sluyters JH (1984) The analysis of electrode impedances complicated by the presence of a constant phase element. J Electroanal Chem 176:275–295
34. Buck RP (1969) Diffuse layer charge relaxation at the ideally polarized electrode. J Electroanal Chem 23:219–240
35. Holze R (2007) Electrochemical thermodynamics and kinetics, in Landolt–Börnstein: numerical data and functional relationships in science and technology, subvol 9A. Springer, New York
36. Morrison SR (1980) Electrochemistry at semiconductor and oxidized metal electrodes. Plenum Press, New York
37. Gerisher H (1969) Charge transfer processes at semiconductor–electrolyte interfaces in connection with problems of catalysis. Surf Sci 18:97–122
38. Okamoto G (1973) Passive film on 18-8 stainless steel structure and its function. Corros Sci 13:471–489
39. North RF, Pryor MJ (1970) The influence of corrosion product structure on the corrosion rate of Cu–Ni alloys. Corros Sci 10:297–311
40. Blundy R, Pryor M (1972) The potential dependence of reaction product composition on copper–nickel alloys. Corros Sci 12: 65–75
41. Druska P, Strehblow HH (1996) A surface analytical examination of passive layers on Cu/Ni alloys: part II. Acidic solutions. Corros Sci 38:1369–1383
42. Badawy WA, Ismail KM, Fathi AM (2009) The influence of the copper/nickel ratio on the electrochemical behavior of Cu–Ni alloys in acidic sulfate solutions. J Alloy Compd 484:365–370
43. Hummel RE, Smith RJ (1988) The passivation of nickel in aqueous solutions—III. The passivation of Ni-30 wt% Cu alloys as studied by in situ electrochemical and optical techniques. Corros Sci 28:279–288
44. Magaino S (1997) Corrosion rate of copper rotating-disk-electrode in simulated acid rain. Electrochim Acta 42:377–382
45. Rice-Jackson LM, Horanyi G, Wieckowski A (1991) Radiotracer study of adsorption of HSO^{-4} and SO_2^{-4} ions on a smooth copper electrode in acid and neutral media. Electrochim Acta 36: 753–757
46. Badawy WA, Ismail KM, Fathi AM (2004) The influence of Ni content on the stability of copper–nickel alloys in alkaline sulphate solutions. J Appl Electrochem 34:823–831
47. Da Cunha Belo M, Hakiki N, Ferreira M (1999) Semiconducting properties of passive films formed on nickel-base alloys type alloy 600: influence of the alloying elements. Electrochim Acta 44:2473–2481
48. Sikora E, Macdonald DD (2002) Nature of the passive film on nickel. Electrochim Acta 48:69–77
49. Chao CY, Szklarska-Smialowska Z, Macdonald DD (1982) The passivity of nickel in phosphate solutions. Part II. Effect of solution pH. J Electroanal Chem 131:289–297
50. Trompette JL, Massot L, Vergnes H (2013) Influence of the oxyanion nature of the electrolyte on the corrosion/passivation behaviour of nickel. Corros Sci 74:187–193
51. Boissy C, Alemany-Dumont C, Normand B (2013) EIS evaluation of steady-state of 316L stainless steel passive film grown in acidic solution. Electrochem Commun 26:10–12
52. Gomes WP, Vanmaekelbergh D (1996) Impedance spectroscopy at semiconductor electrodes: review and recent developments. Electrochim Acta 41:967–973
53. Tremillon B (1993) Electrochimie analytique et réactions en solution—tome 2. Masson, Paris
54. Sato N (1998) Electrochemistry at metal and semiconductor electrodes. Elsevier, Amsterdam
55. Bott AW (1998) Electrochemistry of semiconductors. Curr Sep 17:87–91
56. Petit JP, Antoni L, Baroux B (1993) Polarisation and pH effects on the semiconducting behaviour of passive film formed in chloride containing aqueous solution. In: Proceedings European symposium on modifications of passive films. EFC publications, Paris

57. Darowicki K, Krakowiak S, Slepski P (2006) Selection of measurement frequency in Mott–Schottky analysis of passive layer on nickel. Electrochim Acta 51:2204–2208
58. Olefjord I, Wegrelius L (1990) Surface analysis of passive state. Corros Sci 31:89–98
59. Yang WP, Costa D, Marcus P (1994) Chemical-composition, chemical-states, and resistance to localized corrosion of passive films on an Fe–17%Cr alloy. J Electrochem Soc 141:111–116